International Journal of Greenhouse Gas Control 5 (2011) 1140–1148

Contents lists available at ScienceDirect

International Journal of Greenhouse Gas Control

journal homepage: www.elsevier.com/locate/ijggc

Review

Temporal variations in near-wellbore pressures during CO_2 injection in saline aquifers

Roland T. Okwen[a,*], Mark T. Stewart[b], Jeffrey A. Cunningham[c]

[a] Schlumberger Cambridge Research, High Cross, Madingley Road, Cambridge CB3 0EL, United Kingdom
[b] Department of Geology, University of South Florida, 4202 East Fowler Ave., Tampa, FL 33620, USA
[c] Department of Civil and Environmental Engineering, University of South Florida, 4202 East Fowler Ave., Tampa, FL 33620, USA

ARTICLE INFO

Article history:
Received 10 September 2010
Received in revised form 20 July 2011
Accepted 21 July 2011
Available online 12 August 2011

Keywords:
Anisotropy
Buoyancy
Carbon capture and storage
Permeability
Pressure history

ABSTRACT

Numerical simulations of carbon dioxide injection, via a fully penetrating well, into a homogeneous confined saline aquifer were conducted using TOUGH2 to study temporal variations in near-wellbore pressures. The effect of contrasts in fluid properties on near-wellbore pressure was studied by comparing the predicted pressure histories of carbon dioxide injection to that of water injection into a confined saline aquifer. Simulation results predict an initial jump followed by subsequent decline in near-wellbore pressure over time under isotropic and weakly anisotropic conditions due to phase separation between the less dense and highly compressible carbon dioxide-rich (gas) phase and weakly compressible brine. Conversely, near-wellbore pressure increased monotonically during water injection because the differences between the viscosities, densities, and compressibilities of resident brine and water are relatively small. Sensitivity studies on the effects of the compressibility and viscosity of carbon dioxide and permeability anisotropy suggest that temporal variations in near-wellbore pressures depend strongly on the contrast in density between carbon dioxide and brine, and on the ratio between vertical and horizontal permeabilities of the aquifer (permeability anisotropy). These results suggest that the monitoring near-wellbore pressures during carbon dioxide injection is crucial for maintaining the integrity of the caprock and thereby warrants geomechanical studies.

Contents

1. Introduction

During carbon dioxide (CO_2) injection in confined formations, the integrity of the seals or caprocks, especially the upper confining bed, is pivotal in minimizing risk of potential leakage into overlying environmentally sensitive formations, potable water aquifers for example, and subsequent discharge into the atmosphere. CO_2 leakage from target storage formations during the injection phase could be from pre-existing fractures and faults, leakages at the wellbore

* Corresponding author. Present address: Illinois State Geological Survey, Prairie Research Institute, University of Illinois at Urbana-Champaign, 615 East Peabody Drive, MC-650, Champaign, IL 61820, USA. Tel.: +1 217 244 2869.
E-mail address: rokwen@isgs.illinois.edu (R.T. Okwen).

1750-5836/$ – see front matter
doi:10.1016/j.ijggc.2011.07.011

Nomenclature

Dimensionless parameters and constants

Γ_L	fractional length of pore bodies
λ	pore geometry parameter
ϕ	fraction of original porosity
P_0	strength coefficient
S_{lr}	irreducible saturation of liquid phase
S_{gr}	irreducible saturation of gas phase
S_l	saturation of liquid phase
S_{ls}	liquid phase saturation at which capillary pressure vanishes
k_{vh}	permeability anisotropy ratio, $k_{vh} = k_v/k_h$

Variables

t	time (years)
σ	effective stress (bar)
σ_3	minimum principal stress (bar)
σ_3'	minimum effective principal stress (bar)
σ_v	vertical or overburden stress (bar)
k	intrinsic permeability (m^2)
k_v	permeability in vertical direction (m^2)
k_h	permeability in horizontal direction (m^2)
$P_w(t)$	near-wellbore pressure (bar)
P_{init}	initial pressure (bar)
P_{cap}	brine capillary pressure (bar)
Q	mass injection rate (kg/s)
r	radial distance from injection well (m)

due to improper installation, abandoned wells, or induced fracturing (Nordbotten et al., 2004). Induced fracturing refers to formation fracturing caused by an excessive increase in pore pressure via fluid injection (Martinez et al., 1992). This paper focuses on the temporal variations in maximum pore pressure as a parameter or metric for evaluating the likelihood of fracturing to occur. Since formation pressures are highest at the wellbore during injection, the study of temporal variations in pressure near injection wells is warranted.

Simulations of continuous CO_2 injection into a homogeneous and isotropic confined saline aquifer via vertical wells using a 1-D radial geometry predict monotonic increases in near-wellbore pressures over time ($P_w(t)$) (Pruess et al., 2004). However, a similar simulation using 2D radial geometry (r, z) predicts a decline in $P_w(t)$ at early times (in years). The major difference between the above-mentioned simulations is that the former neglects flow in the vertical direction (vertical flow) as a result of the differences in fluid properties (density and viscosity) between brine and CO_2 while the latter does not. As a result, one may be tempted to conclude that the differences in the near-wellbore pressure histories between the two simulations is due to phase separation. A previous study involving underground waste water injection into deep confined saline aquifer predicted monotonic pressure build-up (Hickey and Vecchioli, 1986). Therefore, an investigation or study of why simulations of continuous injection of CO_2 into a confined aquifer do not predict monotonic pressure build-up over time is needed.

This paper investigates temporal variations in near-wellbore pressures during CO_2 injection in a confined aquifer of radial extent much greater than its thickness. A series of numerical experiments were conducted to investigate the following:

1. test the hypothesis that the decline in near-wellbore pressures during CO_2 injection in isotropic confined aquifers is mostly due to the contrast in density between CO_2-rich (gas) and resident brine, referred to as gravity segregation (phase separation or buoyancy) and
2. study the effects of vertical permeability on changes in near-wellbore pressures over time.

2. Background

Injecting fluids into a porous formation results in net increases in pressures around injection wells. If the pressure increases above a threshold value, fracturing may occur. Previous studies have indicated that formation fracturing is caused by pore pressure exceeding the least principal compressive stress (σ_3) of the formation (Fjær et al., 1992; Zoback, 2007). σ_3 is the sum of pore pressure, P_p, and effective least principal stress (σ_3') i.e.,

$$\sigma_3 = P_p + \sigma_3' \tag{1}$$

Generally, the effective stress (σ') of a formation is the pressure acting between rock grains within a formation (Dake, 1978; Fjær et al., 1992; Zoback, 2007). As P_p increases, σ' decreases and vice versa. When the σ_3' vanishes to zero, P_p becomes equivalent to the least principal stress σ_3 and a slight increase in P_p will initiate formation fracturing in the direction perpendicular to σ_3 (Fjær et al., 1992; Zoback, 2007).

Injection of CO_2 into a confined formation will cause a net increase in P_p. A rule of thumb generally employed is that the maximum fluid pressure should not exceed 90% of the overburden pressure (σ_v) to avoid risk of formation fracturing in the vertical direction (Bachu and Adams, 2003), especially if $\sigma_v = \sigma_3$, which is usually the case at shallow depths.

The tendency of injected CO_2 to override resident brine under deep geologic conditions has been attributed to the contrasts in density and viscosity between CO_2-rich (gas) phase and formation brine (Arts et al., 2004; Torp and Dale, 2004; Nordbotten et al., 2005). A schematic representation of CO_2 injection via a vertical well into a homogeneous confined aquifer is shown in Fig. 1. The effects of phase separation or buoyancy on CO_2 sweep efficiency, storage capacity, solubility in brine and fluid flow dynamics within a confined aquifer have been extensively addressed in the technical literature (van der Meer, 1995, 1996; Ennis-King and Paterson, 2002; Bachu and Adams, 2003; Nordbotten et al., 2005; IPCC, 2005; Ozah et al., 2005; Nordbotten and Celia, 2006; Doughty, 2007; Friedmann, 2007; Bachu, 2008; Okwen et al., 2010). However, the effects of phase separation on temporal variations of formation pressure near injection wells have not been fully addressed.

3. Approach

Radial 2-D simulations of CO_2 and water injection, via a fully penetrating well, into a confined saline aquifer were conducted to achieve the objectives of this study. As shown in Table 2, we considered an aquifer with a radius and thickness of 100 km and 100 m, respectively, or an area of about 3.14×10^{10} m^2. The aquifer was discretized into 435 grids in the radial direction and 20 grids in the vertical, making a total of 8700 grid blocks. Grid sizes in the radial direction were logarithmically distributed, with the finest grid closest to the wellbore and coarsest at the lateral boundaries of the model. As a result, majority of the grid blocks are located within a 15 km radius of the injection well. Because the radial extent of the aquifer is most likely to be significantly greater than CO_2 plume extent, boundary effects are considered negligible. To ensure that boundary effects are minimized, grid blocks along the model's boundary were assigned a volume factor of 10^{30}, thereby imposing constant pressures at the lateral boundaries of the aquifer. The aquifer was also considered to be bounded by two impermeable layers at its top and bottom. The temperature of the injected CO_2 in the simulations is assumed close enough to the temperature of the aquifer that the system may be considered isothermal. In practice,

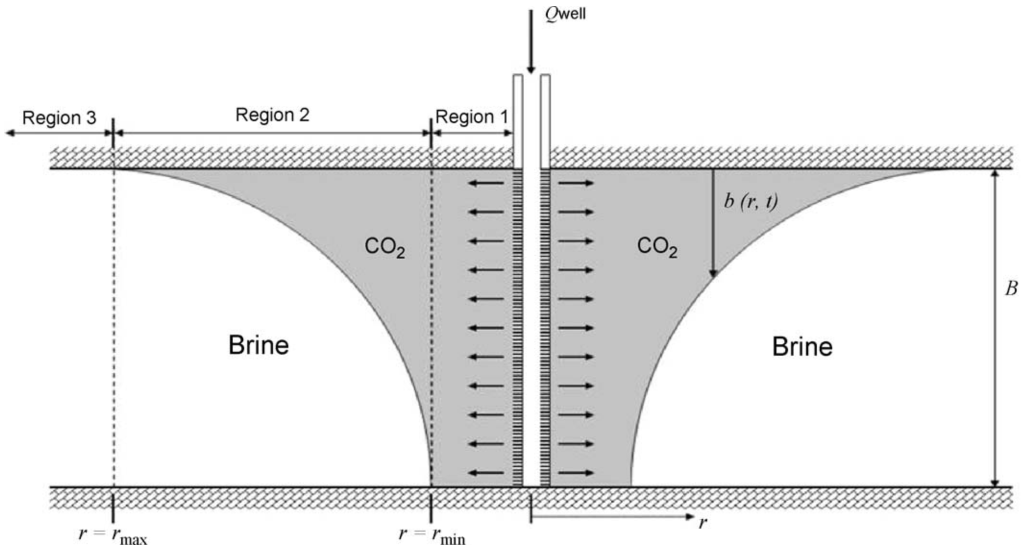

Fig. 1. Schematic representation of CO_2 injection into a confined aquifer via a single vertical injection well. Adapted from Nordbotten et al. (2005).

the difference in temperature between the injected CO_2 and the aquifer could be significant and may also have significant effects on wellbore stability, but those effects are not considered here.

A total of 16 numerical simulations were conducted to test the hypothesis and achieve the objectives stated in Section 1 (see Table 1). These simulations involve CO_2 injection at 100 kg/s at different values of vertical and horizontal permeability. A mass injection of 100 kg/s, for example, is equivalent to the CO_2 emissions from a 288 MWe coal-fired power plant (Hitchon, 1996). Vertical permeabilities ranging from 0.1 to 100 mD and horizontal permeabilities ranging from 10 to 1000 mD were used. Simulations with horizontal permeability less than 10 mD were not considered because formation pressure at or near the injection well exceeded 600 bar, which is the upper limit for the equation of state for CO_2 available in the technical literature (Spycher and Pruess, 2005). Nonetheless, the permeability range considered herein falls within the range of permeability values generally encountered in many sedimentary formations.

The hydrogeologic parameters used in the simulations are listed in Table 2. In Table 2, the symbols S_{lr}, S_{gr}, S_l, λ, P_o, and S_{ls} denote the residual liquid saturation, residual gas saturation, liquid phase saturation, pore geometry parameter, strength coefficient (van Genuchten, 1980), and liquid phase saturation at which P_{cap} vanishes (Pruess and García, 2002). The value of S_{lr} in estimation of capillary pressure (P_{cap}) was set to 0.0 to avoid unrealistic behavior of the van Genuchten (1980) function in which as $k_{lr} \rightarrow 0$, $P_{cap} \rightarrow -\infty$ (Pruess, 1997; Pruess and García, 2002; Müller et al., 2009). The tubes-in-series model developed by Verma and Pruess (1988) was used to account for permeability reduction due to salt (NaCl) precipitation. Γ_L and ϕ_r were both assigned a value of 0.8 in all simulations, similar to what was employed in Code Intercomparison Problem 3 (Pruess et al., 2004). Γ_L represents fractional length of pore bodies and ϕ_r is the fraction of the original porosity at which permeability is reduced to zero (Verma and Pruess, 1988; Pruess and Müller, 2009).

The hypothesis that the decline in near-wellbore pressures during CO_2 injection in isotropic confined aquifers is principally due to contrast in density between CO_2-rich (gas) and resident brine was tested by conducting three numerical simulations with similar aquifer dimensions and input conditions but with different injectants and displaced fluids under isotropic conditions. CO_2, water, and a hypothetical high-viscosity CO_2 (viscous-CO_2) were separately used in each simulation and their temporal changes in

Table 1
Simulations conducted to achieve objectives.

k_v (mD)	k_h (mD)		
	1000	100	10
100	⋆	⋆	–
10	⋆	⋆	⋆
1.0	⋆	⋆	**x**
0.1	⋆	⋆	**x**[a]

$k_v > k_h$ is assumed not feasible. Six additional control simulations were also conducted. They include: (1) water injection, (2) viscous-CO_2 injection, (3) CO_2 injection into a gas-saturated formation, (4) 1-D CO_2 injection, (5) incompressible CO_2 injection, (6) CO_2 injection with permeability and porosity reductions for $k_v = 0.1$ mD, and (7) CO_2 injection with permeability and porosity reductions for $k_v = 100$ mD. $Q = 100$ kg/s.

[a] Maximum pressure in simulation surpassed 600 bar (above pressure limit for CO_2 equation of state used).

Table 2
Input parameters applied in all simulations ($Slr < S_l < 1.0$, and $S_{ls} \approx 1.0$).

Parameter	Value
Dimension $(R \times H)$ m	$10^5 \times 100$
Grid blocks $(X : Z)$	435×20
Wellbore radius (m)	$r_w = 0.3$
Depth (top - bottom) (m)	$D = 1200$–1300
Pore compressibility (Pa^{-1})	$c = 4.5 \times 10^{-10}$
Initial pressure (top-bottom (bar))	$P_{init} \approx 120$–131
Temperature (°C)	$T = 45.0$
Average porosity	$\phi = 0.12$
Average horizontal permeability (mD)	$k = 0.1$–1000
Permeability anisotropy ratio	$k_{vh} = 0.001$–1.0
Simulation time (years)	$t = 150$
Relative permeability	
Brine: van Genuchten (1980)	
$k_{rl} = \sqrt{S^*}\{1 - (1 - [S^*]^{\frac{1}{\lambda}})^{\lambda}\}^2$	$S^* = \frac{S_l - S_{lr}}{1 - S_{lr}}$
Residual brine saturation	$S_{lr} = 0.3$
Exponent	$\lambda = 0.457$
Gas (CO_2): Corey (1954)	
$k_{rg} = (1 - \hat{S})^2 (1 - \hat{S}^2)$	$\hat{S} = \frac{S_l - S_{lr}}{1 - S_{lr} - S_{gr}}$
Residual gas saturation	$S_{gr} = 0.05$
Capillary pressure: van Genuchten (1980)	
$P_{cap} = -P_o([S^*]^{-\frac{1}{\lambda}} - 1)^{1-\lambda}$	$S^* = \frac{S_l - S_{lr}}{S_{ls} - S_{lr}}$
Residual brine saturation	$S_{lr} = 0.0$
Strength coefficient (Pa)	$P_o = 1.96 \times 10^4$
Exponent	$\lambda = 0.457$

Table 3
Initial values of density and viscosity for CO_2, viscous-CO_2, water, and brine.

Fluid	Density (kg/m^3)	Viscosity (Pa s)
CO_2	700	5.6×10^{-5}
Viscous-CO_2[a]	701	8.4×10^{-4}
Water	1000	6.0×10^{-5}
Brine	1100	8.3×10^{-4}

[a] Hypothetical CO_2.

near-wellbore pressures ($P_w(t)$) for periods up to 150 years were compared. Water was chosen as an alternate injectant because the difference between the fluid properties of water and brine is small. Viscous-CO_2 is an unrealistic CO_2 used to test the contribution of viscosity to changes in $P_w(t)$. Viscous-CO_2 is assigned a density and viscosity of 701 kg/m^3 and 8.4×10^{-4} Pa s, respectively. The initial density and viscosity of the resident brine used in all simulations is 1100 kg/m^3 and 8.3×10^{-4} Pa s, respectively. It is worth noting that viscous-CO_2 and resident brine have similar viscosities but significantly different densities. The simulation using CO_2 as the injectant under isotropic conditions is considered as the base case simulation. The mass injection rate and intrinsic permeability (isotropic) applied in the above-mentioned simulations are 100 kg/s and 100 mD, respectively.

A hypothetical simulation of CO_2 injection into a gas (CO_2) saturated formation with initial conditions (temperature and pressure) similar to those of the base case simulation, was conducted as a control experiment. This simulation represents a scenario in which fluid properties of the injected and displaced fluid are similar, like it is the case with water injection into a saline aquifer. Results from this simulation are compared to those of CO_2 and water injection into a saline aquifer to study how differences between the properties of the displacing and displaced fluids impact changes in $P_w(t)$ over time.

The effect of CO_2 compressibility on near-wellbore pressure was studied by conducting a simulation with similar input conditions as the base case simulation, except that the physical properties of CO_2 were kept constant. Constant density and viscosity at initial temperature and pressure (45 °C and 120 bar) conditions, which correspond to about 700 kg/m^3 and 5.57×10^{-5} Pa s, respectively, were applied. Results achieved from this simulation are compared to those of the base case simulation to evaluate the contribution of CO_2 compressibility to changes in pressure around the wellbore.

The physical properties of CO_2 for control simulations, i.e., viscosity and density, were adjusted by editing the "CO2TAB" file in TOUGH2. This file contains tabular data of CO_2 density, viscosity and specific heat enthalpy at different temperatures and pressures (Altunin, 1975; Pruess, 2005). The control simulations conducted herein include injection of viscous-CO_2 and incompressible CO_2.

Effects of vertical permeability on $P_w(t)$ during CO_2 injection were investigated by conducting numerical simulations with anisotropic permeabilities. In the simulations used to investigate the contribution of permeability anisotropy, the vertical permeability (k_v) was varied from 0.1 to 100 mD for a given value of horizontal permeability (k_h) and constant CO_2 mass injection rate (Q). The k_h values of 10, 100, and 1000 mD were employed. Simulations in which $k_v > k_h$ are assumed to be unphysical. We define a permeability anisotropy parameter (k_{vh}) herein as the ratio of the vertical to the horizontal permeability of an aquifer. In Cartesian coordinates (X, Y, Z) vertical k_v is equivalent to permeability along the Z-axis while k_h represent permeabilities along both X- and Y-axes of a grid block. This infers that the permeabilities in the X- and Y-axes are assumed equal. The k_{vh} values considered in this study range from 0.0001 to 1.0.

The TOUGH2 general purpose numerical simulator with the ECO2N fluid property module was utilized to conduct numerical experiments. ECO2N gives accurate fluid properties for water–CO_2–NaCl systems for temperatures ranging between 10 and 110 °C and pressures up to 600 bar (Pruess et al., 1999; Pruess and García, 2002; Pruess, 2004; Pruess and Spycher, 2006, 2007). TOUGH2 was selected because of its widespread usage by many research groups worldwide to solve CO_2 geological sequestration problems (Weir et al., 1995; McPherson and Lichtner, 2001; Ennis-King and Paterson, 2002; Pruess et al., 2003).

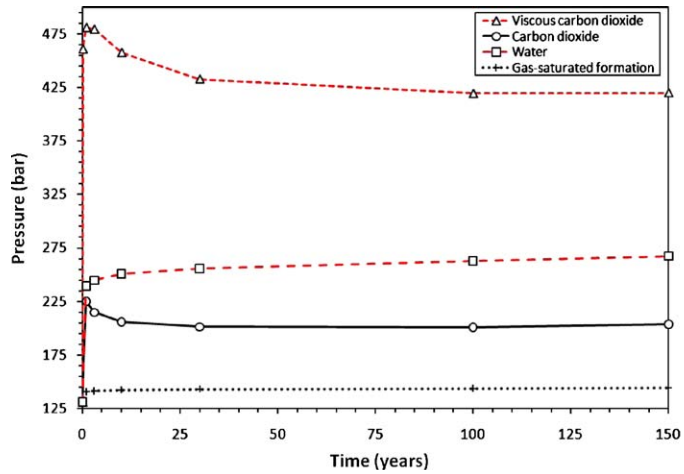

Fig. 2. Effect of density on near-wellbore pressure history at the bottom of the aquifer. Similar trends were observed at the top of the aquifer (Q = 100 kg/s and $k_h = k_v = 100$ mD). Initial pressure at the bottom = 131 bar. The values of density and viscosity of viscous-CO_2 are 701 kg/m^3 and 8.4×10^{-4} Pa s, respectively. Viscous-CO_2 has viscosity equivalent to that of brine (high viscosity) and a density of supercritical CO_2.

4. Results

4.1. Density and viscosity effects

The effect of differences in the physical properties between CO_2 and brine on temporal variations in pore pressure close to the injection well ($P_w(t)$) was investigated by comparing results of CO_2, viscous-CO_2, and water injection into a homogeneous and isotropic confined saline aquifer. Table 3 shows the initial densities and viscosities of CO_2, viscous-CO_2, water, and brine. It can be seen from Table 3 that viscous-CO_2 is as dense as CO_2 and as viscous as brine. A mass injection rate of 100 kg/s and an isotropic intrinsic permeability of 100 mD were applied in the simulations. In the simulation involving injection of viscous-CO_2 into a confined saline aquifer, the density and viscosity of the injectant were kept constant.

Fig. 2 shows changes in $P_w(t)$ over time at the bottom of the aquifer. All the simulations predict an instantaneous pressure jump at the beginning of injection (see Fig. 2). For example, results in Fig. 2 show the $P_w(t)$ for CO_2, viscous-CO_2, and water to increase from 131 bar to about 225 bar, 480 bar, and 240 bar, respectively, after 1 year. These results are in agreement with the findings of Vilarrasa et al. (1988), which suggest that the most likely moment for caprock failure to occur is at the beginning of injection. $P_w(t)$ increases monotonically over time in the simulation that used water as injectant. On the other hand, the CO_2 injection simulation predicts an initial jump in $P_w(t)$ followed by a decline for up to 30 years after which it stabilizes and increases thereafter (t > 100 years). Since the only difference in the input conditions of both simulations is the injectant used, it may be deduced that the difference in the $P_w(t)$ history depicted in Fig. 2 is due to differences between the physical properties of CO_2, water, and brine. However, the differences in the physical properties of water and brine (viscosity and density) are negligible compared to that between CO_2 and brine.

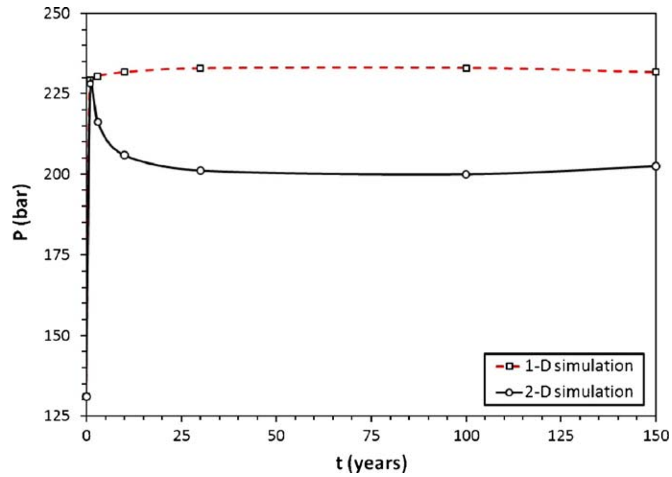

Fig. 3. Near-wellbore pressure (bottom of aquifer) for 1-D and 2-D simulations of CO_2 injection into a confined aquifer (Q = 100 kg/s and $k_h = k_v = 100$ mD).

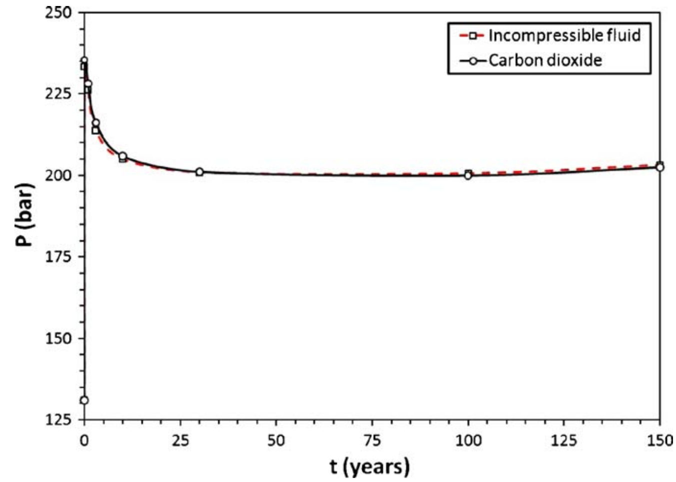

Fig. 4. Effect of CO_2 compressibility on near-wellbore pressure history at the bottom of the aquifer. Similar trends were observed at the top of the aquifer (Q = 100 kg/s and $k_h = k_v = 100$ mD). Initial pressure at the bottom = 131 bar.

Results in Fig. 2 also show $P_w(t)$ for the viscous-CO_2 simulation to increase at early times (for at least 10 years) after which it declines and stabilizes after 100 years of injection. Since viscous-CO_2 and resident brine have equivalent viscosities and different densities, it can be deduced that the decline in $P_w(t)$ between 3 years and 100 years is due to the difference in density between the former and the latter (buoyancy). The minimum difference in density between resident brine and viscous-CO_2 is about 400 kg/m^3. This is because the density of brine would increase during injection, especially at the CO_2–brine interface where CO_2 dissolves into brine and also due to increase in pressure as more fluid is injected into the aquifer. The $P_w(t)$ for viscous-CO_2 is significantly greater than those of CO_2 and water because it has a very high viscosity. A comparison of the $P_w(t)$ histories for CO_2, viscous-CO_2, and water suggest that $P_w(t)$ increases with the viscosity of the displacing fluid, and a decline in $P_w(t)$ over time is influenced by the density difference between the displacing fluid (CO_2, viscous-CO_2, or water) and the displaced fluid (brine).

The $P_w(t)$ history of the simulation of CO_2 injection into a hypothetical gas-saturated formation (Fig. 2) increases monotonically over time. This is because the injected CO_2 has fluid properties similar to the resident gas (CO_2) in the formation. This hypothetical simulation is analogous to water injection into a confined saline aquifer in which both water and brine have similar fluid properties. A comparison of the results in Fig. 2 suggest that $P_w(t)$ increases monotonically when the displacing and displaced fluids have similar densities and viscosities (under isothermal conditions).

A similar study of CO_2 injection into a confined aquifer of infinite radial extent in which vertical flow (buoyancy) is considered negligible (1D radial mesh) predict $P_w(t)$ to increase at early times (Pruess and García, 2002; Pruess et al., 2004) (see Fig. 3). This is because in the 1-D simulation, vertical flow is considered negligible. However, the 2-D simulation results, in which vertical flow (buoyancy driven flow) is taken into account, presented in Fig. 3 depict reduction in $P_w(t)$ at early times, as it is the case with the simulation results present in Fig. 2.

The effect of vertical flow (buoyancy) observed at early times during CO_2 injection into an isotropic and homogeneous saline aquifer can be conceptually described as follows. At the beginning of the injection phase in a CO_2 sequestration project, CO_2 cannot override the resident brine because it has to first displace the brine. As a result, a certain threshold pressure is required to displace the resident brine (Vilarrasa et al., 1988; Müller, 2011). At this stage, lateral viscous flow is dominant while vertical flow (buoyancy) is negligible. As the brine is displaced a separate gas-like phase (CO_2 plume) would occupy the space between the injection well and the CO_2–brine interface. Vertical flow or buoyancy would become important at this point in time because there is room for the gas plume to migrate upwards. As more CO_2 is injected, some of the gas or CO_2 plume would migrate upwards because CO_2 is less dense compared to brine. When a significant volume of the plume accumulates at the bottom of the caprock, the CO_2 plume would override the brine because the former is less viscous. Therefore, the pressure required for a specified flow rate decreases as vertical flow becomes important. In other words, it is easier to push the CO_2 into the aquifer when there is already some compressible and buoyant CO_2 present, versus when there is only brine.

4.2. Effect of CO_2 compressibility

A sensitivity study on the effect of CO_2 compressibility on temporal variations in $P_w(t)$ was achieved by comparing results obtained from incompressible and compressible CO_2 injection simulations (Fig. 4). Results in Fig. 4 indicate that CO_2 compressibility has a negligible effect. This is supported by the results presented in Fig. 5 which shows the changes in water and CO_2 densities over time. It can be deduced from Fig. 5 that the water density

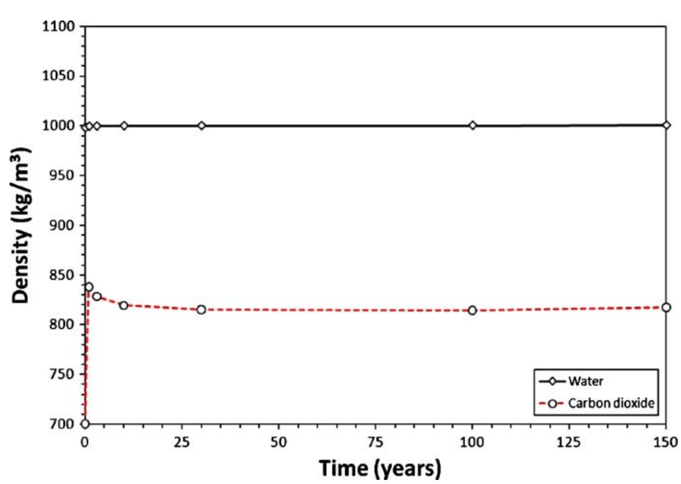

Fig. 5. Temporal variations in CO_2 and water densities (Q = 100 kg/s and $k_h = k_v = 100$ mD). Temporal changes in CO_2 over time ($\Delta\rho_{CO_2}(t)$, $0 \le \Delta\rho_{CO_2}(t) \le 20$ (kg/m^3) is significantly lower than the difference between the densities of water and CO_2 ($\Delta\rho(t)$), $170 \le \Delta\rho(t) \le 200$ (kg/m^3).

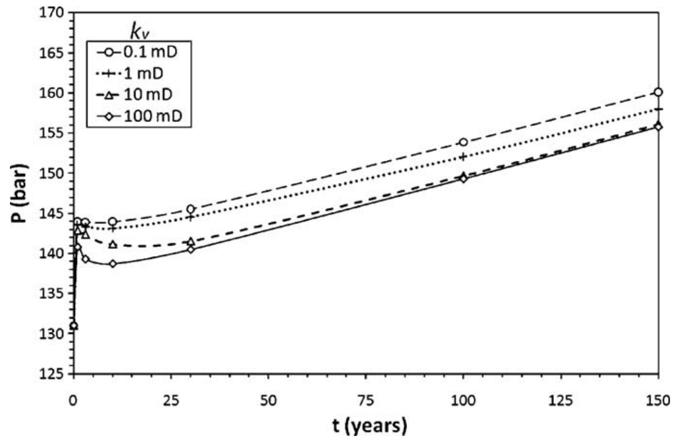

Fig. 6. Effect of k_v on near-wellbore pressure history at the bottom of the aquifer for high k_h values (Q = 100 kg/s and k_h = 1000 mD, $10^{-4} \leq k_{vh} \leq 0.1$).

remains relatively constant over time while that of CO_2 varies over time, especially at early times. However, the difference between the densities of water and CO_2 is significantly greater than temporal changes in the densities of the individual fluids. The predicted $P_w(t)$ of the CO_2 injection case show a slight but noticeable increase after 100 years because as more and more CO_2 is injected into the aquifer over time, it becomes less compressible and more dense near the wellbore.

The simulation results presented in Figs. 2–5 suggest that the decline in $P_w(t)$ at early times (<30 years) of CO_2 injection into a homogeneous and isotropic confined saline aquifer is mostly due to the density difference between CO_2 and brine. This is consistent with the hypothesis that the decline in near-wellbore pressures during CO_2 injection in isotropic confined aquifers is due to contrast between the density of the CO_2-rich (gas) phase and that of resident brine (liquid phase).

4.3. *Effect of vertical permeability, k_v*

The effect of vertical permeability on $P_w(t)$ during CO_2 injection was investigated by comparing $P_w(t)$ histories obtained from simulations with different values of vertical permeability (k_v). Values of k_v used in simulations ranged between 0.1–100 mD. When k_v is very small, fluids within the aquifer preferentially flow in the horizontal direction. This is because as k_v decreases the resistance to fluid flow in the vertical direction increases.

Results from different simulations with k_h values of 10 mD, 100 mD, and 1000 mD and k_v values of 0.1 mD, 1.0 mD, 10 mD, and 100 mD were compared to evaluate the effects of vertical permeability on $P_w(t)$. This makes up a set of numerical simulations conducted for a specified CO_2 injection rate. As depicted in Table 1 the injection rate considered is 100 kg/s. Results from simulations with a k_h value of 1000 mD predict $P_w(t)$ to generally increase monotonically over time as k_v is reduced from 100 mD ($k_{vh} = 0.1$) to 0.1 mD ($k_{vh} = 10^{-4}$) (see Fig. 6). Results in Fig. 6 suggest that both viscous flow and buoyancy are significant at early times (t < 10 years) after which viscous flow is dominant (buoyancy negligible), in formations with k_h equal 1000 mD ($k_{vh} = 0.1$).

On the other hand, results in Fig. 7 show vertical flow (buoyancy) effects to dissipate or become less important as k_h is reduced from 1000 mD to 100 mD, for the same values of k_v considered in Fig. 6, i.e., k_{vh} ranging between 10^{-3} and 1.0. It should be underscored that the main difference between Figs. 6 and 7 is that the minimum and maximum values of k_{vh} of the former is less than that of the latter by an order of magnitude. Results in Fig. 7 show $P_w(t)$ to decrease at early times and subsequently increase at later stages of the simulations, for k_v values greater than 1.0 mD ($k_{vh} > 0.01$). $P_w(t)$ increases monotonically over time at k_v equal to 0.1 mD ($k_{vh} = 0.001$). For example, Fig. 7 shows $P_w(t)$ to decrease over time for k_v values of 10 mD and 100 mD with gravity effect of the latter more pronounce than the former. However, the pressure history of the simulation with k_v equal 1 mD ($k_{vh} = 0.01$) in Fig. 7 show an increase at early times with a slight decline over time. These results indicate under isotropic or weakly anisotropic conditions vertical flow is important and $P_w(t)$ declines over time. However, vertical flow is prevented under anisotropic conditions and hence $P_w(t)$ increases monotonically.

The CO_2 plume evolution over time for the simulation with k_v equal to 1 mD (k_{vh} and Q equal 0.01 and 100 kg/s, respectively) and k_v equal 100 mD ($k_{vh} = 1.0$) in Fig. 7 were closely studied to obtain a possible explanation to the behavior of the $P_w(t)$ history for the former. Figs. 8 and 9 show CO_2 plume distribution at selected times for up 100 years. Fig. 8(a) and (b) depicts a piston-like flow at early times (1 and 10 years) during which vertical flow or buoyancy is less important and viscous flow is dominant. Vertical flow becomes important at large times (e.g. $t \geq 30$ years), when the CO_2–brine interface is far from the injection well. This is marked by phase segregation (gravity or buoyancy) and formation of a "tongue" or thin layer of CO_2 plume beneath the upper confining bed (see Fig. 8(c) and (d)). In addition, separation between CO_2-saturated brine and resident brine, at the CO_2–brine interface (van der Meer, 1996) is also dominant during this period. These findings are in agreement with those of Ennis-King and Paterson (2001) that buoyancy is significant far away from the CO_2 injection well.

A "tongue" of CO_2 plume develops beneath the upper confining bed (phase segregation) at early times (1 year) for the simulation with k_v equal 100 mD ($k_{vh} = 1.0$) (Fig. 9(a)). The distance between the tip of the plume and the injection well increases over time during which the CO_2 plume "tongue" becomes more visible (Fig. 9(a)–(d)). A comparison of the results in Figs. 8 and 9 suggest that the CO_2 plume is well spread across the thickness of the aquifer in Fig. 8 ($k_v = 1$ mD) than in Fig. 9 ($k_v = 100$ mD) due to high resistance to vertical flow in the former. On the other hand, the radial extent of the CO_2 plume after 100 years in Fig. 9 ($k_v = 100$ mD) is greater than that in Fig. 8 because former has a higher k_v value. As a result, vertical flow or buoyancy is enhanced as k_v is increased. The radial extent of the CO_2 plume refers to the distance between the tip of the CO_2 plume and the injection well. Overall, it can be seen from Figs. 8 and 9 that isotropic formations permit gravity segregation, while anisotropic formations suppress gravity segregation.

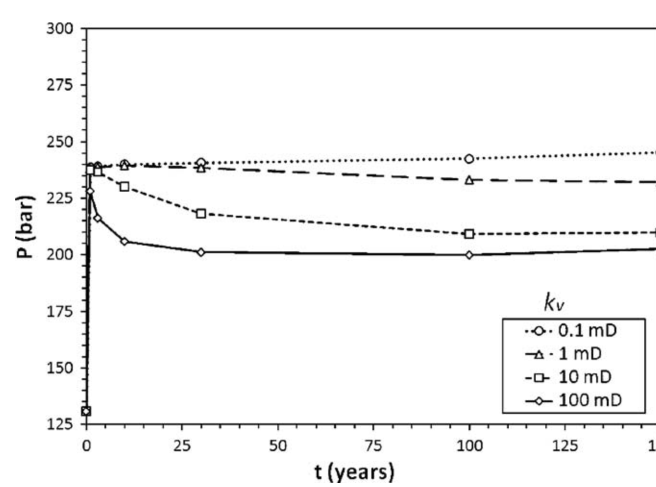

Fig. 7. Effect of k_v on near-wellbore pressures at the bottom of the aquifer as a function of time (Q = 100 kg/s and k_h = 100 mD, $10^{-3} \leq k_{vh} \leq 1$).

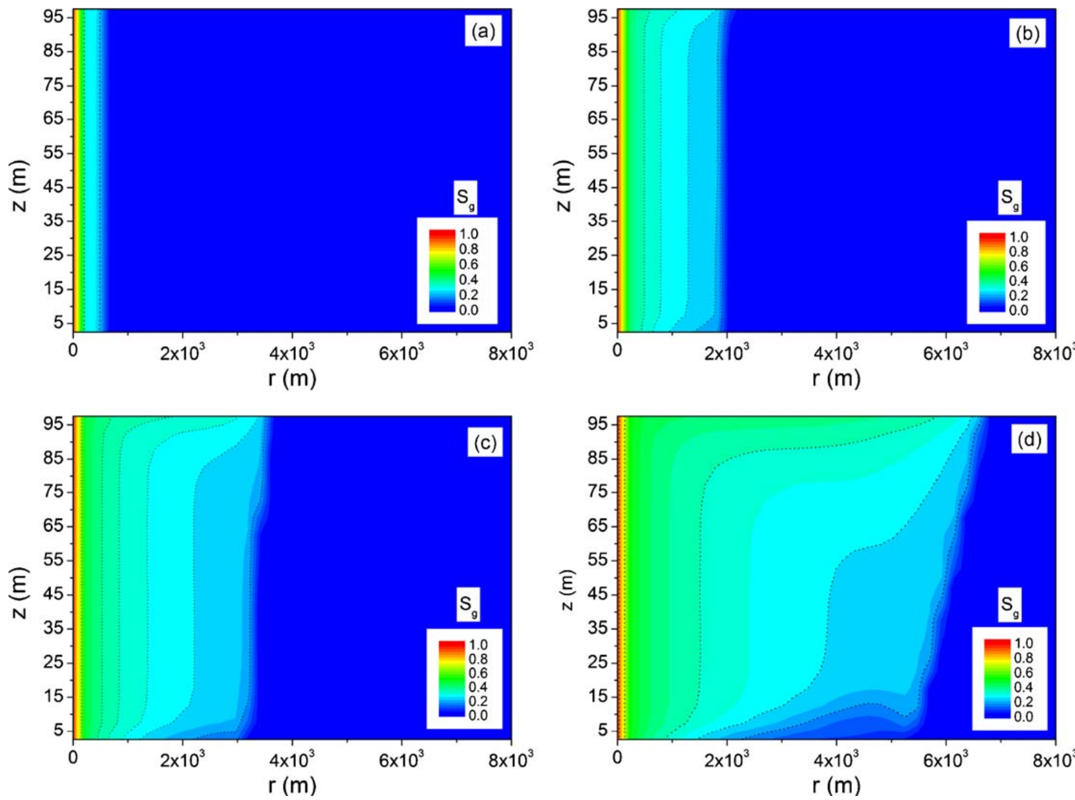

Fig. 8. Gas saturation distribution over time at k_{vh} equal to 0.01 ($k_v = 1$ mD and k_h100 mD). (a) 1 year, (b) 10 years, (c) 30 years, and (d) 100 years. Vertical injection well is positioned at $r = 0.0$ m.

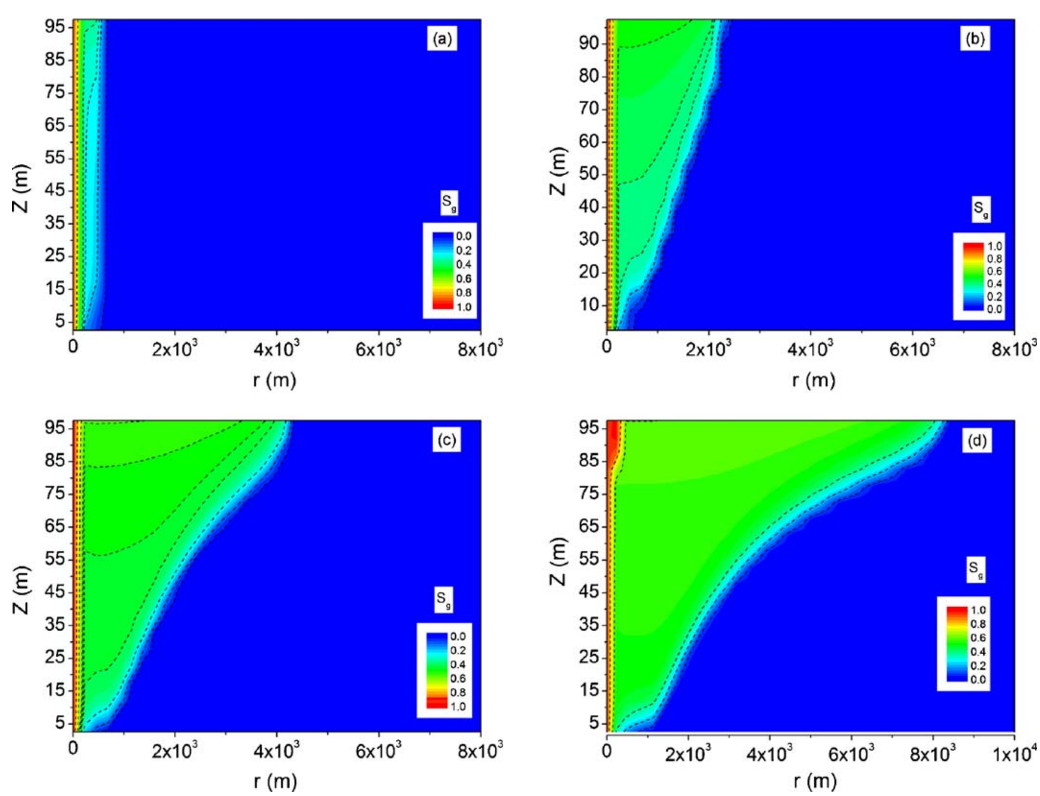

Fig. 9. Gas saturation distribution over time at k_{vh} equal to 1 ($k_v = 100$ mD and k_h100 mD). (a) 1 year, (b) 10 years, (c) 30 years, and (d) 100 years. Vertical injection well is positioned at $r = 0.0$ m.

Table 4
$\Delta P_w(t)$ (bar) as a function of permeability reduction ($k_v = k_h = 100$ mD or $k_{vh} = 1.0$), at the bottom of the formation ($Q = 100$ kg/s).

Time (years)	Permeability reduction		
	Considered	Not considered	Difference
1	94.1	91.0	3.1
3	93.9	80.5	3.4
10	74.7	71.0	3.7
30	70.3	66.2	4.1
100	69.8	65.3	4.5

5. Discussions

Table 1 presents the simulations conducted to achieve the objectives stated in Section 1. The results presented in Figs. 2–5 demonstrate that the decline in $P_w(t)$ at early times during CO_2 injection is mostly due to the difference in density between CO_2 and resident brine. This phenomenon is noticeable in isotropic confined formations where vertical flow or buoyancy effect is significant. Figs. 6 and 7 also demonstrate that $P_w(t)$ strongly depend on k_v. The effect of buoyancy on $P_w(t)$ diminishes as k_v decreases because strong anisotropy suppresses vertical flow.

Vertical flow (buoyancy) and permeability anisotropy can be viewed as competing over control of $P_w(t)$ history during CO_2 injection. The length of time a CO_2 plume at the bottom of an aquifer could take to reach the top increases with decreasing vertical permeability and vice versa (Kumar et al., 2005). This suggests that phase separation between CO_2 and brine is impeded as vertical permeability decreases. Conversely, low vertical permeabilities also impede CO_2-saturated brine at the CO_2–brine interface from sinking by gravity towards the bottom of the aquifer (van der Meer, 1996; Kumar et al., 2005). However, buoyancy eventually predominates CO_2 plume migration far from the injection well (Ennis-King and Paterson, 2002), especially in aquifers having moderately low permeability anisotropy i.e. the k_{vh} value of 0.01 in this study.

To confirm that increases in near-wellbore pressures over time in highly anisotropic aquifers ($k_v = 0.1$ mD) are due to a corresponding increase in the resistance to fluid flow in the vertical direction and not as a result of the salt precipitation (dry-out effect) (Pruess and García, 2002; García, 2003), we conducted control simulations in which permeability and porosity reductions due to salt precipitation are ignored. These simulations were conducted for k_v equal to 0.1 mD and 100 mD. Results of the near-wellbore pressures (P_w) at the bottom of the aquifer for up to 100 years are presented in Tables 4 and 5.

Results in Tables 4 and 5 show pressures to be slightly greater in simulations that account for permeability reductions due to salt precipitation (dry-out effect) than those in which permeability reduction is ignored. These suggest that the effect of permeability reductions due to salt precipitation in the vicinity of the wellbore is significantly low compared to the effect of permeability anisotropy. The salinity used in the simulations conducted herein is 15%. Pressure increases due to salt precipitation may increase at higher values of brine salinity as shown in Pruess and Müller (2009), where 25% brine salinity was employed.

The findings of this study suggest that changes in pressure histories ($P_w(t)$), i.e. pressure decline, in the vicinity of fully completed vertical wells depend strongly on contrasts in density between CO_2 and resident brine during CO_2 injection into isotropic aquifers. However, the decline in $P_w(t)$ diminishes as the aquifer becomes more anisotropic. The degree of formation anisotropy was measured using the formation anisotropy ratio (k_{vh}). Based on the input conditions and parameters used in this study, both vertical flow and the rate at which $P_w(t)$ declines strongly depend on k_{vh}. As k_{vh} decreases from 1.0 (isotropic) to 0.001 (highly anisotropic), both the rate at which $P_w(t)$ declines and vertical flow vanish. Under isotropic conditions, $P_w(t)$ initially jumps to a maximum and subsequently decline over time during CO_2 injection. On the other hand, $P_w(t)$ initially jumps to a value greater than the background and subsequently increases over time at k_v equal to 0.1 mD. Results from this study suggest that the decline in $P_w(t)$ under isotropic conditions may be due to vertical flow of CO_2 (buoyancy driven flow) while the increase in $P_w(t)$ under anisotropic conditions is most probably due to increasing resistance to flow in the vertical direction especially at very small values of k_{vh}.

Results in Fig. 2 also suggest that the total near-wellbore pressure is highly sensitive to the difference in viscosity between the injectant and the displaced fluid. For example, the $P_w(t)$ history of the viscous-CO_2 injection simulation is significantly greater than that of the CO_2 injection (base case) simulation because the former is much more viscous and has viscosity equivalent to that of the displaced fluid (resident brine).

Pressure histories could be used to estimate (1) the maximum pressure and (2) the time after which near-wellbore pressures begin to decline during CO_2 injection in weakly anisotropic aquifers i.e. $k_{vh} > 0.001$. The maximum pressure can then be compared to 90% of the overburden pressure (Bachu and Adams, 2003) to evaluate the risk of possible formation fracturing. The time after which $P_w(t)$ begins to decline can be used as an indicator of the period during which close monitoring of pressure changes at the injection is critical. Pressure monitoring within this period could be pivotal in minimizing risk of undesired formation fracturing.

It should be underscored that variations in near-wellbore pressures may also depend on the absolute or intrinsic permeability, porosity and formation heterogeneity. However, the permeability values considered in this study span the range of permeability values generally encountered in deep geologic formations or reservoirs.

6. Conclusions

Numerical simulations of CO_2 injection into a homogeneous confined saline aquifer were conducted to investigate the root cause or causes of changes in near-wellbore pressures over time. The following conclusions can be made based on results obtained from the numerical simulations;

1. During CO_2 injection into isotropic aquifers, near-wellbore pressures initially increase sharply at the onset of injection, but then decrease slightly over a period of time (≈3 years). The decrease is mostly due to contrast in density between CO_2 and resident brine.
2. Near-wellbore pressures are highly sensitive to viscosity of the injected fluid. Near-wellbore pressures increase as the viscosity of the injectant is increased.
3. In anisotropic formations, temporal changes in near-wellbore pressure histories are more strongly dependent on permeability

Table 5
$\Delta P_w(t)$ (bar) as a function permeability reduction ($k_v = 0.1$ mD and $k_h = 100$ mD or $k_{vh} = 0.001$), at the bottom of the formation ($Q = 100$ kg/s).

Time (years)	Permeability reduction		
	Considered	Not considered	Difference
1	103.3	100.2	3.1
3	104.3	100.8	3.5
10	105.3	101.4	3.9
30	106.3	102.1	4.2
100	108.5	103.8	4.7

anisotropy than on contrast in the properties of the injectant and displaced fluid, in anisotropic formations.

Results from this study indicate that close monitoring of near-wellbore pressure histories during the injection phase of deep geologic storage of CO_2 projects is pivotal. Furthermore, studies of the geomechanical effects on storage formations due to pressure build-up during CO_2 injection are warranted to assure containment.

Acknowledgements

This material is based on work supported by the Florida Energy Systems Consortium (FESC). Financial support has been provided to Roland Okwen by the Alfred P. Sloan Foundation via the National Action Council for Minorities in Engineering (NACME), National Science Foundation (NSF) S-STEM grants(DUE # 0807023 & 0324117), Diverse Student Success (DSS) scholarship at the University of South Florida, and Schlumberger Cambridge Research Ltd. (SCR). Any opinions, findings, conclusions, or recommendations expressed in this dissertation are those of the author and do not necessarily reflect the views of FESC, NSF, USF, the Alfred P. Sloan Foundation, or SCR. The authors also thank William N. Herkelrath of US Geological Survey at Menlo Park, and George Robin of U.S. EPA, San Francisco, for their insights.

References

Altunin, V., 1975. Thermophysical Properties of Carbon Dioxide. Publishing House of Standards, 551 pp.

Arts, R., Eiken, O., Chadwick, A., Zweigel, P., van der Meer, L., Zniszner, B., 2004. Monitoring of CO_2 injected at Sleipner using time-lapse seismic data. Energy 29, 1383–1392.

Bachu, S., 2008. CO_2 storage in geological media: Role, means, status, and barriers to deployment. Progress in Energy and Combustion Science 34, 254–273.

Bachu, S., Adams, J.J., 2003. Sequestration of CO_2 in geological media in response to climate change: Capacity of deep saline aquifers to sequester CO_2 in solution. Energy Conversion and Management 44, 3151–3175.

Corey, A., 1954. The interrelation between gas and oil relative permeabilities. Producers Monthly, 38–41.

Dake, L., 1978. Fundamentals of Reservoir Engineering, vol. 8, 2nd ed. Elsevier Scientific Publishing, Amsterdam.

Doughty, C., 2007. Modeling geologic storage of carbon dioxide: Comparison of non-hysteretic and hysteretic characteristic curves. Energy Conversion & Manangement 48.

Ennis-King, J., Paterson, L., 2001. Reservoir engineering issues in the geological disposal of carbon dioxide. In: Proceedings of the International Conference on Greenhouse Gas Control Technologies, CSIRO, Melbourne, Australia, pp. 290–295.

Ennis-King, J., Paterson, L., 2002. Engineering aspects of geological sequestration of carbon dioxide, Vol. SPE-77809, Asia Pacific Oil and Gas Conference and Exhibition, Melbourne, Australia, October 8–10, SPE and CSIRO Petroleum.

Fjær, E., Holt, R., Horsrud, P., Raaen, A., Risnes, R., 1992. Petroleum related rock mechanics. In: Development in Petroleum Sciences 33, 1st ed. Elsevier.

Friedmann, J., 2007. Geological carbon dioxide sequestration. Elements 3, pp. 197–184, Carbon Management Program, Lawrence Livermore National Laboratory.

García, J.E., 2003. Fluid dynamics of carbon dioxide disposal in saline aquifers. Doctoral dissertation, University of California, Berkeley.

Hickey, J., Vecchioli, J., 1986. Subsurface injection of liquid wastes with emphasis on injection practices in Florida, paper 2281. U.S. Geological Survey, U.S. Geological Survey Water-Supply.

Hitchon, B., 1996. Aquifer Disposal of Carbon Dioxide. Geoscience Publishing Ltd., Sherwood Park, Alberta, Canada.

IPCC., 2005. IPCC special report on carbon dioxide capture and storage. In: Metz, B., Davidson, O., de Coninck, H.C., Loos, M., Meyer, L.A. (Eds.), Prepared by Working Group III of the Intergovernmental Panel on Climate Change, Report, Intergovernmental Panel on Climate Change, Cambridge, United Kingdom and New York, NY, USA.

Kumar, A., Ozah, R., Noh, M., Pope, G.A., Bryant, S., Sepehrnoori, K., Lake, L.W., 2005. Reservoir simulation of CO_2 storage in deep saline aquifers. Society of Petroleum Engineering Journal 9 (SPE89343), 336–348.

Martinez, S., Steanson, R., Coulter, A., 1992. Petroleum Engineering Handbook: Formation Fracturing. Society of Petroleum Engineers, 12 pp. ISBN: 1-55-563-010-3 (chapter 55).

McPherson, B., Lichtner, P., 2001. CO_2 sequestration in deep saline aquifers, Washington, D.C., U.S.A. First National Conference in Carbon Sequestration.

Müller, N., 2011. Supercritical CO_2–brine relative permeability experiments in reservoir rocks—literature review and recommendations. Transport in Porous Media 87, 367–383.

Müller, N., Qi, R., Mackie, E., Pruess, K., Blunt, J., 2009. CO_2 injection impairment due to halite precipitation. Energy Procedia 1, 3507–3514, http://dx.doi.org/10.1016/j.egypro.2009.02.143.

Nordbotten, J., Celia, M., 2006. Similarity solutions for fluid injection into confined aquifers. Journal of Fluid Mechanics 561, 307–327.

Nordbotten, J., Celia, M., Bachu, S., 2005. Injection and storage of CO_2 in deep saline aquifers: Analytical solution for CO_2 plume evolution during injection. Transport in Porous Media 58, 339–360.

Nordbotten, J.M., Celia, M.A., Bachu, S., 2004. Analytical solutions for leakage rates through abandoned wells. Water Resources Research 40, W04204.

Okwen, R.T., Stewart, M., Cunningham, J., 2010. Analytical solution for estimating storage efficiency of geologic sequestration of CO_2. International Journal of Greenhouse Gas Control 4 (1), 102–107.

Ozah, R., Lakshminarasimhan, G., Sepehrnoori, K., Bryant, S.,2005. Numerical simulation of the storage of pure CO_2 and CO_2-H_2S gas mixture in deep saline aquifers. In: SPE Annual Technical Conference and Exhibition, SPE 97255, Society of Petroleum Engineers. Society of Petroleum Engineers, Dallas, TX, USA, pp. 1–12.

Pruess, K., 1997. On vaporizing water flow in hot sub-vertical rock fractures. Transport in Porous Media 28, 335–372.

Pruess, K., 2004. The TOUGH2 code—a family of simulation tools for multiphase flow and transport processes in permeable media. Vadose Zone Journal 3, 738–746.

Pruess, K., 2005. ECO2N: A TOUGH2 Fluid Property Module for Mixtures of Water, NaCl, and Carbon Dioxide. Lawrence Berkeley National Laboratory, Berkeley, CA.

Pruess, K., García, J., 2002. Multiphase flow dynamics during CO_2 disposal into saline aquifers. Environmental Geology 42, 282–295.

Pruess, K., García, J.E., Kovscek, T., Oldenburg, C., Rutqvist, J., Steefel, C., Xu, T., 2004. Code intercomparison builds confidence in numerical simulation models for geologic disposal of CO_2. Energy 29 (9–10), 1431–1444.

Pruess, K., Müller, N., 2009. Formation dry-out from CO_2 injection into saline aquifers: 1. Effects of solids precipitation and their mitigation. Water Resources and Research 45 (w03402), 1–11.

Pruess, K., Oldenburg, C., Moridis, G., 1999. TOUGH2 users' guide, version 2.0, Manual LBNL-43134, Lawrence Berkeley National Laboratory, Berkeley, CA (accessed 10.06.07).

Pruess, K., Spycher, N., 2006. ECO2N—a new TOUGH2 fluid property module for studies of CO_2 storage in saline aquifers. Lawrence Berkeley National Laboratory, Berkeley, CA.

Pruess, K., Spycher, N., 2007. ECO2N - A fluid property module for the TOUGH2 code for studies of CO_2 storage in saline aquifers. Energy Conversion and Management 48 (6), 1761–1767.

Pruess, K., Xu, T., Apps, J., García, J.E., 2003. Numerical modeling of aquifer disposal of CO_2. Society of Petroleum Engineering Journal 8 (1), 49–60.

Spycher, N., Pruess, K., 2005. CO_2–H_2O mixtures in the geological sequestration of CO_2. II. Partitioning in chloride brines at 12 to 100 $^\circ$C and up to 600 bar. Geochimica et Cosmochimica Acta 69, 3309–3320.

Torp, T., Dale, J., 2004. Demonstrating storage of CO_2 in geological reservoirs: the Sleipner and SACS projects. Energy 29.

van der Meer, L.G.H., 1995. The CO_2 storage efficiency of aquifers. Energy Conversion and Management 36 (6–9), 513–518.

van der Meer, L.G.H., 1996. Computer modelling of underground CO_2 storage. Energy Conversion and Management 37 (6–8), 1155–1160.

van Genuchten, M.T., 1980. A closed-form equation for predicting the hydraulic conductivity of unsaturated soils. Soil Science Society of America Journal 44, 892–898.

Verma, A., Pruess, K., 1988. Thermohydrologic conditions and silica redistribution near high-level nuclear wastes emplaced in saturated geological formations. Journal of Geophysical Researches 93 (B2), 1159–1173.

Vilarrasa, V., Bolster, D., Olivella, S., Carrera, J., 1988. Coupled hydrodynamical modeling of CO_2 sequestration is deep saline aquifers. International Journal of Greenhouse Gas Control 4, 910–919.

Weir, G., White, S., Kissling, W., 1995. Reservoir storage and containment of greenhouse gases. Energy Conversion and Management 36 (6–9), 531–534.

Zoback, M., 2007. Reservoir Geomechanics. Cambridge University Press, Cambridge, United Kingdom. ISBN: 978-0-521-77069-9.